

# Near-infrared imaging and structured light ranging for automatic catheter insertion

Vincent Paquit<sup>a,b,c</sup>, Jeffery R. Price<sup>a</sup>, Ralph Seulin<sup>b</sup>, Fabrice Mériaudeau<sup>b</sup>,  
Ruby H. Farahi<sup>a,c</sup>, Kenneth W. Tobin<sup>a</sup> and Thomas L. Ferrell<sup>c</sup>

<sup>a</sup> Oak Ridge National Laboratory<sup>†</sup>, P.O. Box 2008, MS-6010, Oak Ridge, TN 37831-6010, USA;

<sup>b</sup> Le2i, University of Burgundy, 12 rue de la fonderie, 71200, Le Creusot, FRANCE;

<sup>c</sup> Department of Physics and Astronomy, University of Tennessee, Knoxville, TN 37996-1200, USA

## ABSTRACT

Vein localization and catheter insertion constitute the first and perhaps most important phase of many medical procedures. Currently, catheterization is performed manually by trained personnel. This process can prove problematic, however, depending upon various physiological factors of the patient. We present in this paper initial work for localizing surface veins via near-infrared (NIR) imaging and structured light ranging. The eventual goal of the system is to serve as the guidance for a fully automatic (i.e., robotic) catheterization device. Our proposed system is based upon near-infrared (NIR) imaging, which has previously been shown effective in enhancing the visibility of surface veins. We locate the vein regions in the 2D NIR images using standard image processing techniques. We employ a NIR line-generating LED module to implement structured light ranging and construct a 3D topographic map of the arm surface. The located veins are mapped to the arm surface to provide a camera-registered representation of the arm and veins. We describe the techniques in detail and provide example imagery and 3D surface renderings.

**Keywords:** imaging, vein, near-infrared, range analysis, structured light, venous imaging

## 1. DESCRIPTION OF PURPOSE

Development of technologies that enable automated insertion of needles and catheters will clearly play a vital role in the operating room of the future. One vision for future operating rooms is a clean room environment void of any humans beyond the patient. Subsequently, future operating environments will require remote and autonomous insertion of intravenous (IV) catheters in a patient without the assistance of a nurse. To reach our goal, we focus our work on finding the best way to reproduce the two main actions of this medical procedure with a robot:

1. Localizing the best target subcutaneous vein. The “golden rule” in nursing for IVs is to use the largest vein and the smallest gauge catheter possible. Image processing algorithms combined with an illumination and camera acquisition system using the absorption/reflection properties of light in tissues will allow us to choose the target vein.
2. Computing the path for the needle that has to enter the skin with at a specific angle. By obtaining a 3D model of the surface of the skin and adding to this model a mapping of the target veins, we will be able to guide the needle into the vein. This path will be computed only if we know the position of the patient compared to the position of the robot in a 3D space.

---

Further author information: (Send correspondence to V.P.)  
V.P. : E-mail: paquitvc@ornl.gov, Telephone: 1 865 241 3302

<sup>†</sup>This paper was prepared by the OAK RIDGE NATIONAL LABORATORY, Oak Ridge, Tennessee, 37831-6285, operated by UT-BATTELLE, LLC for the U.S. DEPARTMENT OF ENERGY under contract DE-AC05-00OR22725.

## 2. METHODS AND SYSTEM

### 2.1. Methods

Previous research has been completed to characterize the propagation of light in tissue as a function of wavelength [1]. A good example of this light interaction is apparent from viewing through the skin where red blood appears blue [2]. In the near-infrared part of the light spectrum, the light penetrates deeper into the tissue and is less sensitive to the pigmentation of the skin. To use the non-invasive characteristics of NIR light, we have designed a ring of NIR light emitting diodes (LED) with seven different wavelengths to illuminate the scene. This lighting system allows us to detect and separate veins from other tissues.

For the 3D reconstruction process, we use active optical triangulation, a well known method for acquiring range data [3]. This method is based on the combination of a structured light laser source and a camera. After calibration of the system, the depth of each point of the laser line is triangulated and the 3D points are calculated from a 2D projection. These points are then gathered into a 3D point cloud corresponding to the surface of the skin.

Combining the 3D and 2D information, we will compute the 3D position of the target vein and determine an optimum path for the needle.

### 2.2. Experimental setup

Our acquisition system (Figure 4) is composed of a NIR video camera with a 740nm long-pass interferometric filter, a NIR multi-wavelength ring of LEDs and a NIR line-generating laser module.

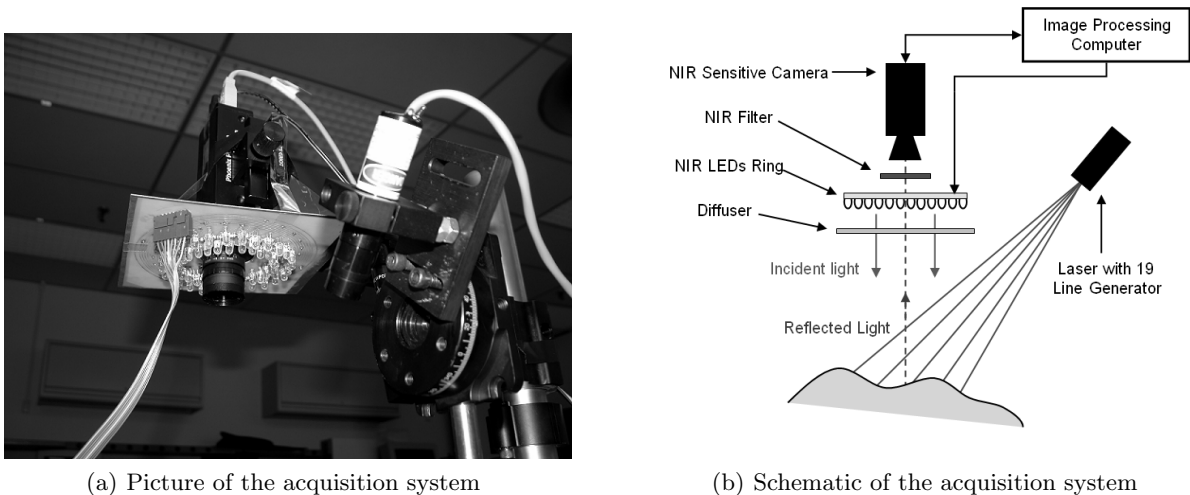


**Figure 1.** Picture and schematic of the acquisition system including a NIR sensitive camera, a NIR interferometric filter, a NIR multi-wavelength ring of LEDs and a NIR line-generating laser module. The diffuser has been removed from the setup (a) to show the ring of LEDs.

We have selected a Mutech Phoenix PC-1280/M Monochrome Camera with 8 or 10 bit pixel formats supporting both VGA and SXGA resolutions running respectively at 60 and 15 frames per second (fps). Our choice was based on the appropriate spectral response of the CMOS sensor in the NIR range of light (Figure 2), its compactness and the communication protocol allowing both video signal transfer and hardware configuration. The camera is connected and controlled by an IBM compatible personal computer (PC) via a USB 2.0 connection. The video resolution has been set to  $640 \times 480$  (VGA) at 60 fps taking into account:

- the processing speed needed: A nurse is able to take a decision based upon the unpredictable movements of patients, so we need to have the same possibility of reaction. Considering that the human eye transmits at least 20 images per second to analyze the movement in a scene, we set the lower processing time limit at 25 frames per second. This speed will be the minimum allowed to take a decision on the real time needle path computation with our image processing algorithms. In this paper we present a two steps analysis of the scene by switching

between the two light sources (laser line generator / ring of LEDs). So, of these 60 frames, half of them are used for the 3D reconstruction (3.2) and half for the localization of the target veins (4).

- the maximum size of eventual artifact : The size of the smallest viewable element is inversely proportional to the resolution of the picture for a given scene. By using a lower resolution we want to limit the presence of artifacts in the images like for example the detection of capillary or perturbations caused by hairs (i.e., unwanted light reflection of the laser lines, high absorption of NIR light comparable to the veins).

The optical system is composed of a 25mm lens with a NIR interferometric filter on it. In our setup the NIR filter is used as a high pass filter; combined with the spectral response of the camera we obtain a band pass filter which allows a sensitivity in the spectral range going from 740nm to 960nm.

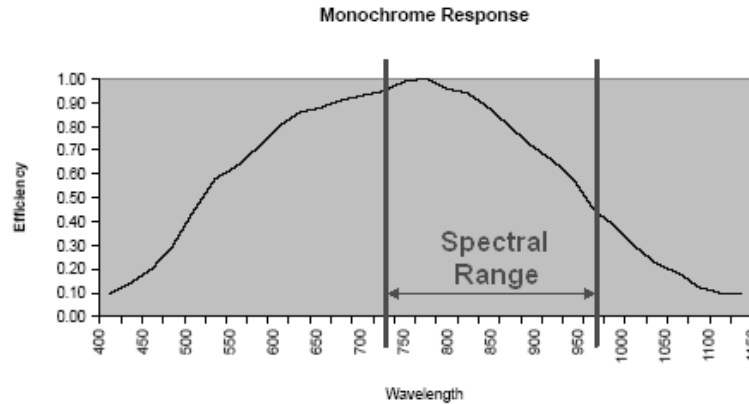


**Figure 2.** Sensor Spectrum Response (Without IR filter) and limits of the spectral range used in our experiment.

The lighting source is composed of 56 LEDs mounted on a ring with eight LEDs for each of the seven wavelengths (740, 770, 810, 840, 880, 910 and 950nm). Each LED has a power dissipation around 30mW. The position of the LEDs on the ring has been determined to get a uniform illumination of the scene even by switching or combining the different wavelengths. In addition we have placed a diffuser in front of the LEDs to increase this uniformity. A wide range of NIR LEDs has been used to enhance the contrast between the veins and the skin. Past studies on the propagation of light in biological tissues examined the relations between the nature of tissue and the absorption of light (blood [2], water [4], skin [5], fat [6]). Through this research we are investigating wavelength and wavelength combinations that will provide optimum contrast between near-surface veins and tissue. With a Measurement Computing PMD-1024HLS which is a 24-line digital I/O module connected to the computer, we can select a wavelength or a combination of wavelengths used to illuminate the scene.

We use a 19-line generating beam splitter mounted on a 785nm laser diode to generate the structured light source needed to create the 3D triangulation system. With the 19-line generator, we plan to cover a surface up to eight square inches, therefore providing flexibility and control of the robotic catheter insertion system.

### 3. CALIBRATION AND 3D RECONSTRUCTION

#### 3.1. Acquisition System Calibration

In computer vision, the calibration of an optical system is used to determine the intrinsic and extrinsic parameters of a camera [7]. These parameters correspond to the mathematical relations between the 3D space of reference and the 2D perception of the scene. With the resulting equations, we are able to correct the distortion of the picture and to compute the metric value of a pixel. Different methods of calibration already exist and many tend to use the same process [7, 8]; we used the method describe in [9] for our application. The calibration is made when the position of the laser compared to the camera and the focal plane of the optical system have been fixed. The method consists of taking pictures of different orientations of a planar checkboard pattern considered

as a metric reference for our system. Notice that we have to illuminate the scene with the NIR lighting source due to the presence of the interferometric filter. The analysis of the position of all the square corners in a set of six to ten pictures give us the intrinsic parameters of the camera: focal length, principal point, skew coefficient, radial and tangential distortions. The Figure 3 presents an example of the correction result obtained with these parameters.

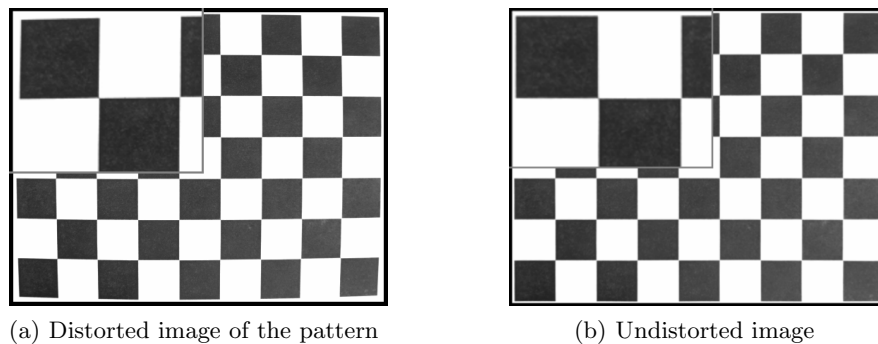
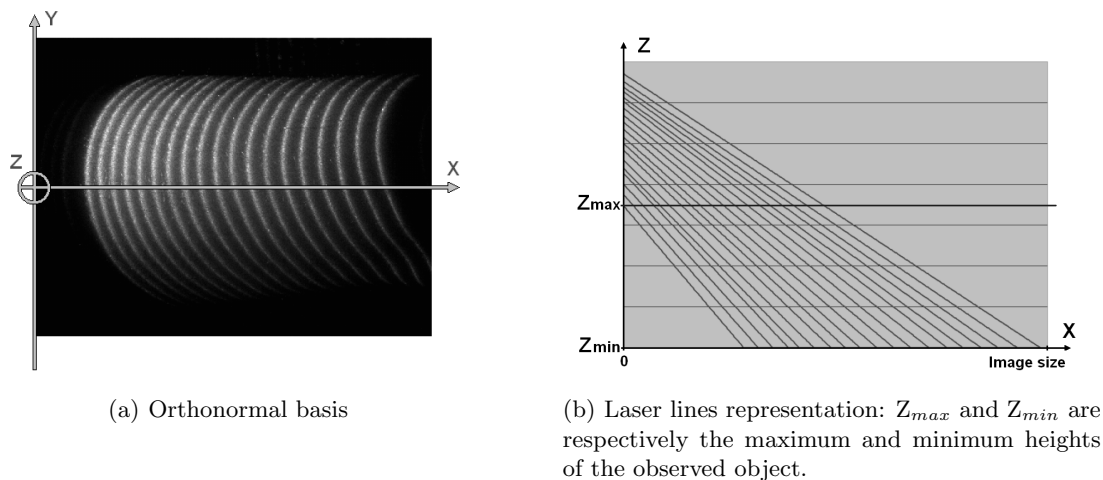


**Figure 3.** Distorsion correction example

In addition to the distortion correction, this method offers the possibility to calculate the metric coordinates of a pixel depending on the position of the image plane along the optical axis ( $Z$  axis in Figure 4). Placing the checkboard pattern at two or more planes perpendicular to the optical axis while visualizing the projection of the laser stripes on the pattern, we are able to determine a relation between the dimensions of the pattern and the position of the laser lines. In addition, by combining these multi-level relations we are able to compute the linear equations of the laser lines for a given value of  $y$  (Figure 4(b)). Assuming that after correction of the distortions, all the lasers lines projected on a plane perpendicular to the optical axis are parallels independently to the projection plane and are projected orthogonally to the  $X$  axis by setup, we are able to define the position of each pixel of the laser stripe lines in the 3D baseline by a linear equation where the only variable is the  $x$  coordinate of the same pixel in the 2D image because  $y$  is a constant due to the orthogonality of the laser lines with  $X$ .



(a) Orthonormal basis

(b) Laser lines representation:  $Z_{max}$  and  $Z_{min}$  are respectively the maximum and minimum heights of the observed object.

**Figure 4.** Calculation of the laser line equations after calibration of the system

### 3.2. 3D Reconstruction

The 3D reconstruction process uses active optical triangulation by combining a camera and a laser stripe line generator [3]. The geometry of the laser triangulation is shown in Figure (5). The camera is aligned along the

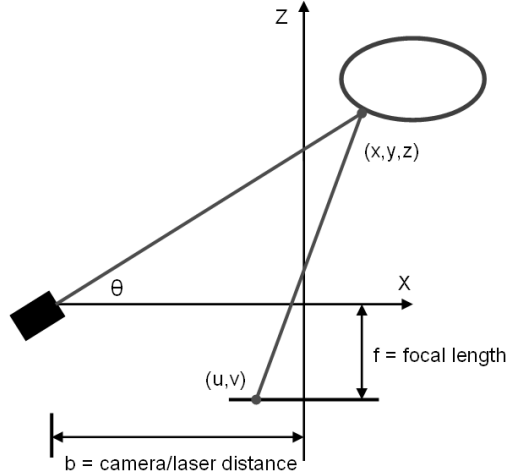


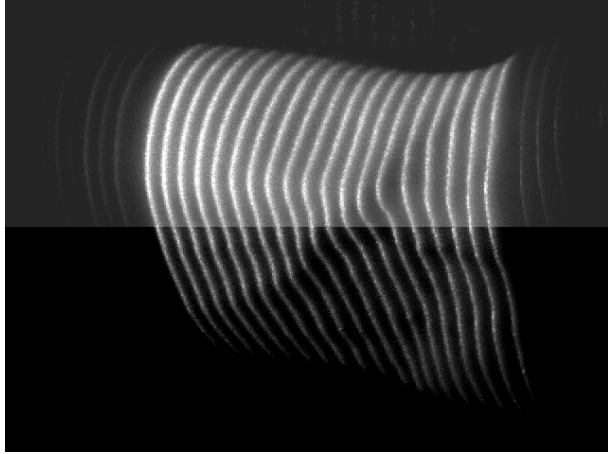
**Figure 5.** Principle of 3D reconstruction with active optical triangulation

Z axis and the laser line generator is positioned at a distance  $b$  from the camera with the angle  $\theta$  relative to the X axis. Assuming that the considered laser point coordinates  $(x, y, z)$  in the 3D baseline has a projection  $(u, v)$  on the image plane, the similar triangles equations give the mathematical relation between the measured quantities  $(u, v, \theta)$  and the coordinates  $(x, y, z)$ :

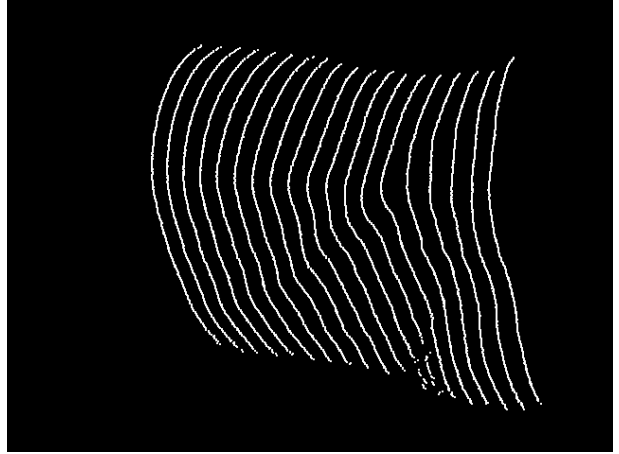
$$[x, y, z] = \frac{b}{f \cdot \cot \theta - u} [u, v, f]. \quad (1)$$

The calculation of the equation of each of the stripe lines during the calibration process depend on the triangulation equation above. Because the position of the laser compared to the camera is fixed, the equation are calculated only one time. The second part of the 3D reconstruction process depends on the detection of the center of the laser stripe lines. The reflection of the laser light on the surface of the skin is comparable to a blurry Gaussian signal. To detect with accuracy the position of the center of the laser line, we have tested three subpixel peak detection algorithms: Blais and Rioux [10], Forest [11] and the center of mass. In each case a pre-processing slicing filter was used to remove the additional lines generated by the laser diode and to remove additive noise from the picture (Figure 6(a)). In almost all the tests, the best results were obtained with the Forest algorithm with a 6th order filter (Figure 6(b)). A classification of each of the center line pixels is performed to associate them with one of the nineteen laser lines, considering the possibility of missing points in the 3D point cloud. Due to the approximate local linearity of the skin surface we fill the holes in our 3D mesh by linear interpolation based on the direct neighborhood of the missing points. The resulting association pixel-line number will determine the linear equation used for the 3D reconstruction (Figure 6(c)).

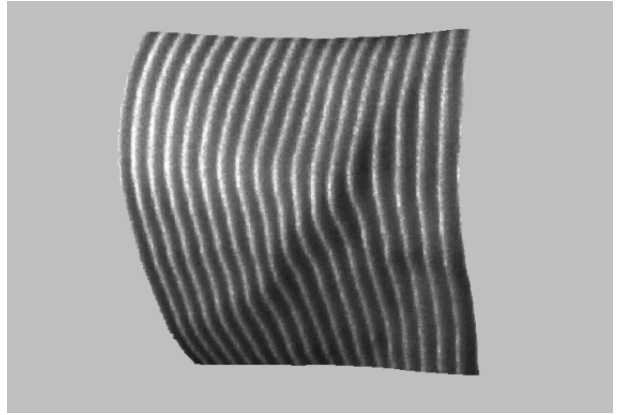
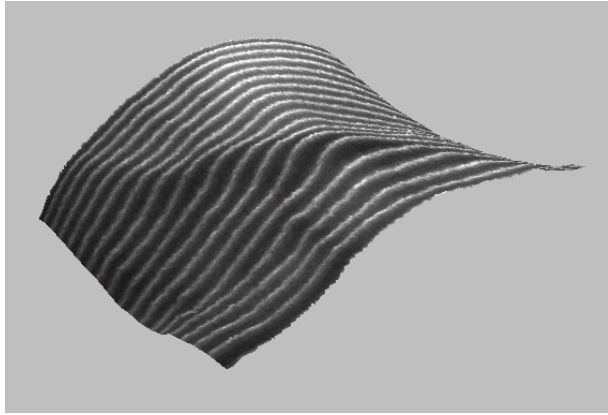
The 3D modeling of the scene is computed in real time at 30 frames per second. The complete mesh of the scene is generated during this period of time but for visualization only. In reality the interesting information we want to extract concerns the venous area. Indeed, we plan to use the 3D position of the vein for a robotic catheterization and a robot need only the parametric curve of the path to be able to stick the vein. So we only need to compute the 3D model of the surface of the skin around the target veins. Usually in a picture, the ratio veins/skin is about 30% in maximum which implies a processing time divided at least by three if we generate the 3D mesh in the area of interest.



(a) Slicing pre processing result: the upper half part presents the raw image and the lower half part the processing result



(b) Stripe line peak detection. Notice the presence of a hole in the lower right part which will be corrected during the 3D mesh generation.



(c) 3D reconstruction with laser stripe lines texture mapped on it

**Figure 6.** 3D reconstruction steps and perspectives visualisations

#### 4. VEIN DETECTION AND NEEDLE PATH CALCULATION

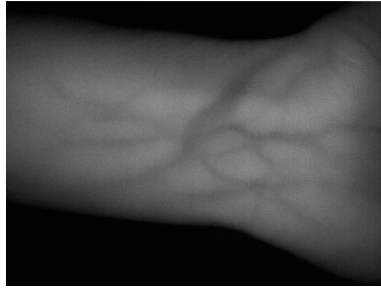
The next step of our work consists of finding the optimum vein for catheterization. Assuming that we have to use the largest vein and the smallest gauge catheter possible, we have implemented image processing algorithms to find the largest vein in the scene compared to the size of a needle.

We previously explained why our NIR light source creates a contrast enhancement between skin and veins regardless the color of the skin. Due to these absorption-reflection phenomena, we have a NIR image with light and dark areas corresponding respectively to the skin and to the veins (and hairs). We present in Figure (7(a)) an example of an unprocessed image of a wrist acquired with our vision system. Despite the uniformity of our lighting source one may notice a difference of illumination and contrast between the middle and the borders of the picture. This characteristic is due to the topography of the surface of the skin. Indeed the incidence angles between the rays of light and the surface of the skin condition the quantity of light reflected to the camera. This difference of illumination is considered as a leak of energy due to the high scattering medium observed. A compensation of this loss is made by acquiring the reflected light from a uniform white lambertian surface which is still bright in the NIR range and use it as a reference for the illumination correction [12] and of course enhance the contrast in the dark areas. Assuming that  $I_{init}(x, y)$  is the initial image (Figure 7(a)),  $I_{illum}(x, y)$  is the illumination reference image (Figure 7(b)) and  $I_{result}(x, y)$  is the resulting image (Figure 7(c)), the illumination

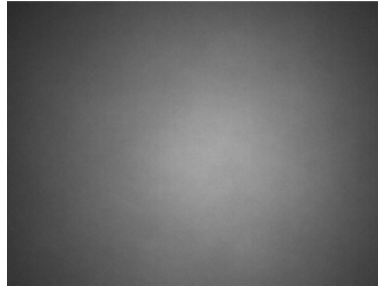
correction given by the equation 2 is presented figure 7:

$$I_{result}(x, y) = \frac{I_{init}(x, y)}{I_{illum}(x, y)} \times C. \quad (2)$$

where  $C$  is a scaling coefficient dynamically determined to restore the eight bits coding of the grey pixel values.



(a) Acquisition of a wrist before the image processing



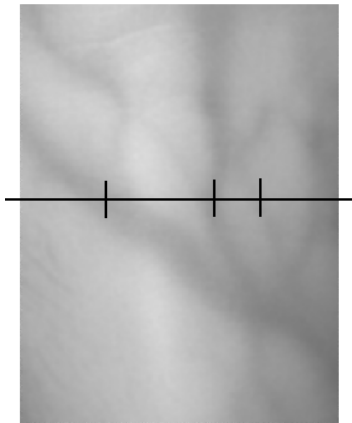
(b) Grayscale picture of the illumination of a white sheet of paper



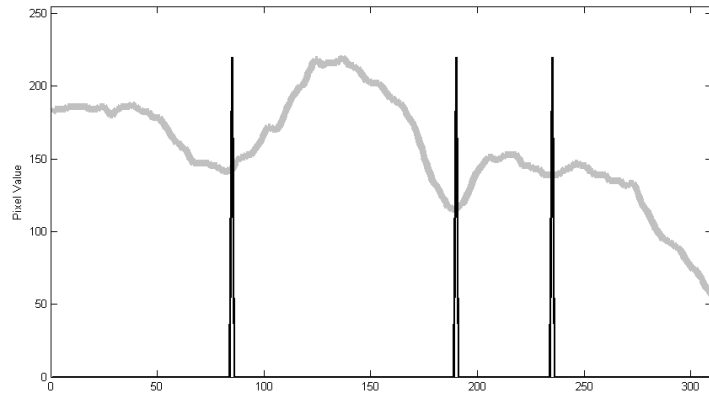
(c) Result of the illumination correction of the scene

**Figure 7.** Illumination correction process

Recall that the detection of the veins by the human eye is made by finding the transitions between light and dark areas. This method is quite similar to the one we used to detect the center of the laser stripe lines in 3.2. But in this case we have to detect the position of minima instead of maxima in a picture with an unknown number of veins and with significant noise. Assuming that the lighting source and the illumination correction allow a good contrast enhancement, we use a basic grayscale simplification of the image with a median filter [13] to reduce the influence of the additional noise and increase the impression of transition between two groups of gray level pixels. After simplification, we use a combination of a 2nd and 6th order filter to detect the minima in the rows and the columns of the picture. In figure 8(b) we present the result of the local minima detection for the black marked row in figure 8(a). A black cross was added to locate the position of each minima in the picture .



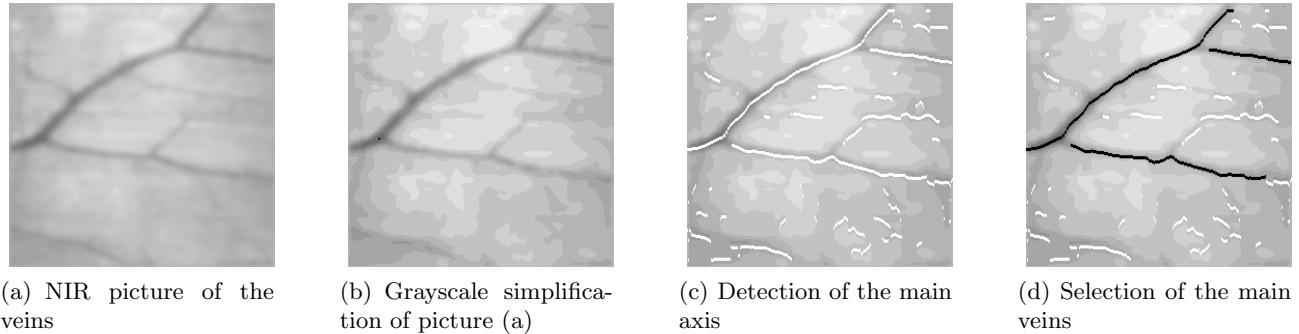
(a) NIR image of veins before the image processing



(b) Detection of the center point of the veins for the row selected in Figure 8(a)

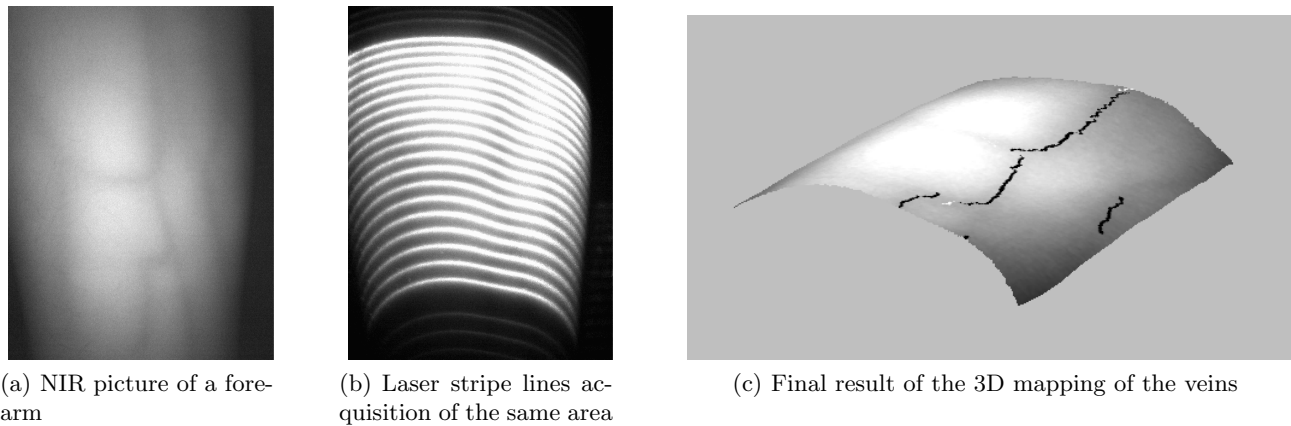
**Figure 8.** Veins detection principle

Figure 9 shows our process on an image starting with the acquisition of the subcutaneous veins with our NIR system. After illumination correction and grayscale simplification (Figure 9(b)) we apply the vein detector for each row and each column of the picture (Figure 9(c)). At the same time, we are gathering information about the pixel detected and its neighborhood like the local width of the vein or topographic data and compiling a blob coloring [14]. During this process we will detect other elements considered as veins (eg., hairs, artefact detection,...). In a final step we will use the gathered information and the rule of the nurses to select only the path with the most linear part and the largest veins (Figure 9(d)).



**Figure 9.** 4 steps needed to find the best possible target veins in the picture.

The next phase is the combination of the 3D information obtained in 3.2 and the 2D localization of the target veins. We present in figure 10 a complete example of the mapping of the target veins on the 3D model of a forearm.



**Figure 10.** Mapping of the detected vein on a 3D model of a forearm

With these results we are able to compute a 3D path for the robot which is characterized by three points: (1) guide the needle to the surface of the skin, (2) give a correct inclination to the needle according to the angle of penetration required, and (3) give a correct orientation based on the main axis of the vein.

## 5. CONCLUSION AND FUTURE WORK

In this paper, we present how NIR imaging can be used to find vessels under the skin and show how combined with image processing algorithms it is possible to get 3D information about the subcutaneous veins. Finally, we demonstrate the efficiency of a non-invasive and easy to use technique and we also present a possible application of our work by automatically guiding a catheter to administer an IV. In a next phase of this project we are

going to improve the efficiency of our device. With our lighting system, we encountered some difficulties in the creation of contrast to enhance or detect veins under certain conditions. The increase of power dissipation of the LEDs and the adjunction of polarizer filters will allow better control of the illumination of the scene and a better study of the tissue reflection and absorption properties. In addition new image processing algorithms will be implemented to solve this problem with a different approach [15]. Information missing in our 3D model concerns the depth of the veins. Because the propagation of light in tissue follows the radiative transport equation [16] it will be possible to find a relation between the quantity of light absorbed by a vein and its surrounding tissues and its depth. With these improvements we plan to compute the exact 3D position of subcutaneous veins instead of their location compared to the surface of the skin.

## REFERENCES

1. T. Vo-Dinh, *Biomedical Photonics Handbook*, CRC Press, Boca Raton, 2003.
2. A. Kienle, R. Hibst, R. Steiner, L. Lilge, I. A. Vitkin, B. C. Wilson, and M. S. Patterson, "Why do veins appear blue? A new look at an old question," *Applied Optics* **35**, pp. 1151–1160, mar 1996.
3. P. J. Besl, *Surfaces in range image understanding*, Springer-Verlag New York, Inc., New York, NY, USA, 1988.
4. G. Hale and M. Querry, "Optical constants of water in the 200-nm to 200-micrometer wavelength region," *Appl. Opt.* **12**, pp. 555–, 1973.
5. C. R. Simpson, M. Kohl, M. Essenpreis, and M. Cope, "Near-infrared optical properties of ex vivo human skin and subcutaneous tissues measured using the Monte Carlo inversion technique," *Physics in Medicine and Biology* **43**(9), pp. 2465–2478, 1998.
6. J. Conway, K. Norris, and C. Bodwell, "A new approach for the estimation of body composition: infrared interactance," *Am J Clin Nutr* **40**(6), pp. 1123–1130, 1984.
7. J. Heikkila and O. Silven, "A Four-step Camera Calibration Procedure with Implicit Image Correction," in *CVPR '97: Proceedings of the 1997 Conference on Computer Vision and Pattern Recognition (CVPR '97)*, p. 1106, IEEE Computer Society, (Washington, DC, USA), 1997.
8. Z. Zhang, "Flexible Camera Calibration by Viewing a Plane from Unknown Orientations," in *ICCV*, pp. 666–673, 1999.
9. J.-Y. Bouguet, *Camera Calibration Toolbox for Matlab*.
10. F. Blais and M. Rioux, "Real-time numerical peak detector," *Signal Process.* **11**(2), pp. 145–155, 1986.
11. J. Forest, J. M. Teixidor, J. Salvi, and E. Cabruja, "A Proposal for Laser Scanners Sub-pixel Accuracy Peak Detector," in *Workshop on European Scientific and Industrial Collaboration*, pp. 525–532, (Mickolj (Hungria)), May 2003.
12. R. K. G. Klančar, M. Kristan, "Wide-angle camera distortions and non-uniform illumination in mobile robot tracking," *Int. Journal of Robotics and Autonomous Systems* **46**(2), pp. 125–133, 2004.
13. Y. Lee and S. Kassam, "Generalized Median Filtering and Related Nonlinear Filtering Techniques," *ASSP* **33**, pp. 672–683, 1985.
14. D. H. Ballard and C. M. Brown, *Computer Vision*, Prentice Hall Professional Technical Reference, 1982.
15. N. Miura, A. Nagasaka, and T. Miyatake, "Feature extraction of finger-vein patterns based on repeated line tracking and its application to personal identification," *MVA* **15**, pp. 194–203, October 2004.
16. A. D. Kim, "Transport theory for light propagation in biological tissue," *Optical Society of America Journal A* **21**, pp. 820–827, May 2004.